HHS Public Access

Author manuscript

*Semin Nucl Med*. Author manuscript; available in PMC 2017 January 01.

Published in final edited form as:

*Semin Nucl Med*. 2016 January ; 46(1): 28–39. doi:10.1053/j.semnuclmed.2015.09.004.

# The Potential of Metabolic Imaging

**Valentina Di Gialleonardo**[1], **David M. Wilson**[2], and **Kayvan R. Keshari**[1,†]

[1]Department of Radiology and Molecular Pharmacology and Chemistry Program Memorial Sloan Kettering Cancer Center (MSKCC), New York, NY 10065, USA

[2]Department of Radiology and Biomedical Imaging University of California San Francisco (UCSF), San Francisco, California, 94158 USA

## Abstract

Metabolic imaging is a field of molecular imaging that focuses and targets changes in metabolic pathways for the evaluation of different clinical conditions. Targeting and quantifying metabolic changes non-invasively is a powerful approach to facilitate diagnosis and evaluate therapeutic response. This review addresses only techniques targeting metabolic pathways. Other molecular imaging strategies, such as affinity/receptor imaging or microenvironment-dependent methods are beyond the scope of this review. Here we describe the current state of the art in clinically translatable metabolic imaging modalities. Specifically, we will focus on positron emission tomography (PET) and magnetic resonance spectroscopy (MRS), including conventional $^{1}H$ and $^{13}C$ MRS at thermal equilibrium and hyperpolarized magnetic resonance imaging (HP MRI). In this paper, we first provide an overview of metabolic pathways that are altered in many pathological conditions and the corresponding probes and techniques used to study those alterations. We will then describe the application of metabolic imaging to several common diseases including cancer, neurodegeneration, cardiac ischemia, and infection/inflammation.

## 1. Introduction

Metabolism refers to a set of enzyme-catalyzed biochemical reactions that take place within cells to maintain homeostasis. These reactions are organized into metabolic pathways, which are finely regulated by enzyme concentrations and catalytic efficacy as well as cofactor concentrations. In the clinic, several non-invasive imaging techniques have been developed to identify altered metabolic pathways characteristic of a variety of diseases.

Positron emission tomography (PET) and proton magnetic resonance spectroscopy ($^{1}H$-MRS) represent the majority of current non-invasive imaging techniques used to follow metabolism *in vivo*. With PET, it is possible to visualize the accumulation of radioactive molecules in a specific tissue or organ, with the anatomic location confirmed using

†Correspondence and Reprint Request: Kayvan R. Keshari, Ph.D. Assistant Member, Department of Radiology and Molecular Pharmacology and Chemistry Program, Memorial Sloan Kettering Cancer Center, 1275 York Avenue, New York, NY 10065, Phone: (646) 888-3631, Fax: (646) 422-0247, rahimikk@mskcc.org.

coregistered computed tomography (CT) or magnetic resonance imaging (MRI). The most widely utilized PET metabolic probe has been [$^{18}$F]fluoro-deoxyglucose ([$^{18}$F]FDG), which is accumulated in highly glycolytic tissues. The main advantages of PET are that it is easy to perform, incredibly sensitive and provides reasonable spatial resolution (approximately 5mm isotropic for PET), although it suffers from lack of specificity due to the inability to resolve different radioactive molecules non-invasively. Magnetic resonance spectroscopy imaging (MRSI), like PET, is a technique that allows the detection of metabolites spatially resolved *in vivo*, but without the use of ionizing radiation. For example, for brain MRSI, using long echo time (TEs) it is possible to visualize choline (Cho) used to evaluate membrane turnover and proliferation, creatine (Cr) for tissues energetics, N-acetylaspartate (NAA) for mitochondria and neuronal integrity, and lactate for anaerobic metabolism. Using short TEs, it is possible to identify additional metabolites; myo-inositol, glutamate, glutamine and glycine. $^{1}$H MRSI can be obtained in 10-15 minutes and, is therefore, easily incorporated into a routine imaging clinical study minimizing discomfort to the patient.[1, 2] One of the limitations of this technique is low sensitivity, with metabolite concentrations required to be on the order of mM.

For the most part, patient MRS exams have used $^{1}$H, though despite technical challenges, there has also been considerable interest in using $^{13}$C magnetic resonance spectroscopy imaging ($^{13}$C MRSI) to study of the backbone of organic compounds in specific tissues. The MRI-detectable nucleus $^{13}$C accounts for only 1.1% of molecular carbon and thus renders thermal equilibrium $^{13}$C MRSI limited for rapid study of endogenous $^{13}$C. To increase sensitivity and increase spectral resolution, isotopically enriched molecules are infused and $^{13}$C spectroscopy is performed, often with $^{1}$H decoupling.[3-5] These enriched compounds are virtually identical to the parent compound and typically provide no appreciable isotope effect in the time scale of the experiment. Infusions can raise the concentration of $^{13}$C upwards of $10^{3}$ to $10^{4}$ fold and therefore the metabolism of these molecules may be studied without background contamination of endogenous pools.[6] In contrast to PET, which can quantify the dynamic flux of radioactive probes over time, the most widely implemented MRS methodologies estimate metabolite concentrations at steady state.[7]

Another emerging non-invasive technique that is rapidly growing as a molecular imaging methodology is hyperpolarized MRI (HP MRI). HP MRI allows the detection of $^{13}$C-enriched molecules with a signal increased several orders of magnitude (up to $10^{7}$) in comparison to conventional spectroscopy. With this technique it is possible to follow single and multiple metabolic pathways using one or a combination of several HP probes. The great advantage of this technique is that after the injection, it is possible to follow in real-time the conversion of a substrate to its metabolic products, whereas PET can only detect the incorporation of radiolabeled probes in a tissue without distinguishing the parent compound from the formed radiolabeled product.[8, 9] HP MRI, could then, overcome the limitations of conventional $^{1}$H and $^{13}$C MRSI and provide complimentary information to PET studies in the future.

In the following sections, the main metabolic pathways with respective probes designed to target those pathways are described in detail.

### a) Glycolysis

Is a 10-step metabolic pathway that takes place in the cytosol of cells and predominantly oxidizes glucose to pyruvate, resulting in increased ATP and NADH.[10] Glucose is taken up from a range of glucose transporters (GLUTs), comprised of 14 isoforms with specific expression pattern, substrate specificity and kinetics.[11, 12] In mammalian cells, after entering the cell glucose is typically converted by hexokinase to glucose-6-phosphate (G6P). G6P has the potential to then continue into the glycolytic pathway, ending in the formation of pyruvate or it can leave glycolysis and enter the pentose phosphate pathway (PPP), which is essential for the regulation of the redox status as well as ribose synthesis. Glycolysis can also be altered in several pathological conditions and targeting cellular transport and early metabolism has been the subject of extensive PET and MRSI research. [$^{18}$F]FDG PET is a powerful clinical tool able to evaluate the upstream glycolytic pathway non-invasively. [$^{18}$F]FDG is transported efficiently into the cells by GLUT transporters and in the cytosol is phosphorylated by Hexokinase II to [$^{18}$F]FDG-6-Phosphate and is trapped in the cell. [$^{18}$F]FDG-6-P can be dephosphorylated by glucose-6-phoshatase (G6P) and then released into the extracellular space.[13] This tracer has been used successfully for a variety of human diseases, but primarily for cancer diagnosis and therapy follow-up. Several other applications in neurology and cardiology have been described. While [$^{18}$F]FDG has remarkable sensitivity, lack of specificity can present a diagnostic problem. One approach to improving specificity and identifying specific metabolites has been the use of $^{13}$C agents. In order to study glycolysis, $^{13}$C glucose has been used to follow $^{13}$C, both at steady state and using dynamic HP studies. Additionally, with $^{1}$H MRI it is possible to detect some products of glycolysis, including pyruvate. Moreover, HP [1-$^{13}$C] pyruvate has been developed to study the formation of HP lactate *in vivo*. This conversion is particularly relevant to cancer, for which a high rate of glycolysis is observed.

### b) Tri-carboxylic acid (TCA) cycle

In normoxia, the two carbons of the acetyl moiety of acetyl-CoA are predominantly derived from glycolytic flux. The formation of acetyl-CoA is catalyzed by pyruvate dehydrogenase (PDH) by the ligation of acetyl group to coenzyme A. Under hypoxic conditions, the flux from glucose to citrate decrease and the acetyl-CoA is mainly directed towards fatty acid biosynthesis.[14] Because acetate acts as a key player in both pathways, [$^{11}$C] acetate has been developed to study its incorporation noninvasively using PET. [$^{11}$C]Acetate is taken up by the monocarboxylate transporter (MCTs) and then converted in [$^{11}$C]acetyl-CoA by a mitochondrial enzyme, acetyl CoA synthetase (ACSS). [$^{11}$C]acetyl-CoA as described above can either enter TCA cycle or be addressed into fatty acid metabolism.[15, 16] Because of its versatility, [$^{11}$C] acetate has been employed in several areas of medicine and research as a non-invasive tool, including cardiology and oncology.[16] Analogously, in $^{13}$C NMR spectroscopy, infusions of [2-$^{13}$C] acetate have been used to follow metabolic flux non-invasively as well as hyperpolarized [1-$^{13}$C] acetate.[17-21] Hyperpolarized [2-$^{13}$C] pyruvate can be used to follow the downstream TCA cycle. Pyruvate is converted to acetyl-coenzyme A (acetyl-CoA) by pyruvate dehydrogenase (PDH). Acetyl-CoA then enter the TCA and then further $^{13}$C label downstream to the TCA intermediate, such as [1-$^{13}$C]citrate and [5-$^{13}$C]glutamate.[22]

### c) Choline metabolism

Cho is an essential constituent of cells and mitochondrial membranes, and an important precursor of the neurotransmitter acetylcholine (Ach). Because of its ubiquitous presence, Cho can affect both signaling and metabolic pathways.[23] High levels of Cho intermediates and enzymes in Cho metabolism are observed during cell transformation, tumor growth and invasion.[24, 25] Phosphocholine and total Cho, as well choline kinase-alpha (ChoKα), phosphatidylcholine-specific Phospholipase D and C are overexpressed in activated cancer cells and, therefore, suggests Cho and its metabolites as potential targets for molecular imaging.[24] [$^{18}$F] fluorocholine and [$^{11}$C]choline are PET tracers developed to target this pathway. Additionally, pool size measurements using $^{1}$H-MRSI of total Cho provide a possible approach to assess turnover and proliferation.

### d) Creatinine metabolism- the Creatine Kinase (CK)/Phosphocreatine (PCr)/Creatine (Cr) system

Cr is a nitrogenous organic intermediate derived from arginine, methionine and glycine. Upon phosphorylation, it is mainly utilized to supply energy to tissues, in particular muscle. In tissues with high energy demands, such as the heart and brain, the transport from ATP production sites (mitochondria) requires an efficient system for transport, namely *CK/PCr/Cr*.[26, 27] Cr levels are often used in $^{1}$H-MRS to assess tissue energetics. This analysis can be supplemented by less sensitive approaches to measure PCr and ATP, such as $^{31}$P spectroscopy.[28, 29]

### e) Amino acid metabolism

Here we present a few examples, which highlight the general direction of metabolic imaging of amino acid metabolism.

**Glutamine/glutamate—**L-glutamine is an essential amino acid important for cell survival and proliferation. It can be metabolized through multiple pathways and a precursor of proteins, amino sugars, purines/pyrimidines and nucleic acids. Glutamine is the most abundant extra cellular amino acid (0.7mM) whereas glutamate, the immediate metabolite of glutamine, is most abundant intracellularly (2-20mM).[30, 31] Several radioactive probes labeled with different isotopes have been produced for PET imaging to visualize glutamine/glutamate metabolism; ([$^{18}$F](2S,4S)-4-(3-fluoropropil)glutamine, [$^{18}$F](2S,4R)-4-(3-fluoropropil)glutamine and L-[5-$^{11}$C]- glutamine), which is mostly used for visualizing glutaminolysis in tumors not detected by [$^{18}$F]FDG.[32-35] Labeled [$^{13}$C] glutamine has been used in normal $^{13}$C MRS as well in hyperpolarized MRI, in order to follow the glutamine-derived metabolites *in vivo*.[36-38] HP [5-$^{13}$C] glutamine has been used *in vitro* to detect glutaminase activity in human hepatocellular carcinoma.[36] A recent paper from Canapè et al., describes the possibility to follow glutaminolysis in prostate cancer cells before and after anticancer treatment. First, they show a linear correlation between more glutaminolytic phenotype and cell proliferation detected by HP [5-$^{13}$C] glutamine. Moreover, use of this HP probe allowed the possibility to follow the efficacy of drug treatment.[39]

**Methionine, one carbon metabolism—**Methionine is a sulfur-containing amino acid essential for the biosynthesis of proteins. Methyl groups derived from this cycle are the

major source of post-translational modification methylation metabolism of proteins and comprise an important role in epigenetic alterations.[40] L-methyl-$^{11}$C-methionine has been synthesized and used routinely in PET for cancer imaging.[41, 42] Typically, the role of $^{11}$C-methionine is in imaging an increase in protein synthesis and this has been predominantly applied to the study of high grade brain tumors. The use of $^{11}$C-methionine though has been limited to sites with cyclotrons onsite due to the short half-life of $^{11}$C, though it has provided a useful alternative when standard $^{18}$F-FDG PET is difficult to use.

## 2. Cancer imaging

Cancer is a heterogeneous group of diseases characterized by uncontrolled cell growth and spread of transformed cells from the organ of origin. In 2015, more than 1,658,370 new cases are expected to be diagnosed with more than 500,000 people expected to die of the disease. After heart disease, cancer is the second leading cause of death in US.[43] In the past 25 years, the link between cancer and metabolism has become a subject of increased interest with atypical metabolism now recognized as an important hallmark of cancer.[44] While normal resting cells use predominantly fatty acid oxidation and glucose oxidation to produce ATP, cancer cells shift their metabolism to meet the higher bioenergetics demands. One of the most characteristic phenomena seen in cancer cells is the Warburg effect.[45, 46] Cancer cells shift from oxidative phosphorylation to aerobic glycolysis. Most of the glucose that enters the glycolytic pathway is therefore converted to lactate, rather than metabolized in the mitochondria by the TCA cycle.[45, 47] Another well-known metabolism alteration in cancer cells is altered glutamine uptake and metabolism. Glutamine after entering the cell is metabolized to α-ketoglutarate, an important intermediate that can feed the TCA cycle.[48] Cancer cells not only increase their catabolism, but also their anabolic metabolism for macromolecule biosynthesis, such as proteins, lipids, and nucleotides. The unbalanced reactive oxygen species (ROS) production resulting from cell transformation and changed metabolism is countered by production of macromolecules, which are able to quench ROS and allow these cells to maintain redox homeostasis.[49, 50]

### a) FDG PET and radiolabeled amino acids

[$^{18}$F]FDG is one of a handful of FDA approved PET tracers and undoubtedly the most applied tracer for cancer diagnosis, staging and treatment follow-up.[51] FDG PET is a semi-quantitative approach, widely used in clinical practice for lymphoma staging and solid tumor imaging such as lung, breast, colorectal, head and neck cancer imaging.[51-53] FDG PET is of limited use in prostate cancer imaging due to the proximity of the prostate to the urinary tract, it's route of excretion.[54] [$^{11}$C]choline and [$^{18}$F]fluorocholine have been applied in prostate cancer imaging with contradictory results, thus, making localized prostate cancer metabolic imaging by PET a difficult target.[55]

Due to increased protein synthesis in cancer cells, several radiopharmaceuticals based on amino acid analogues have been produced. L-methyl- $^{11}$C-methionine is the one of the more promising radiotracers used in the evaluation of tumors using PET (MET PET). It has been successfully used for the detection and staging of brain tumors, especially glioblastoma. Using this tracer is possible to differentiate high grade to low grade glial neoplasms.[56] A recent paper by Venneti et al., describes the potential of radiolabeled glutamine analogues

for the metabolic evaluation of gliomas *in vivo*. [$^{18}$F]FDG shows a selective high uptake in progressive glioma but not in neuroinflammation, suggesting that this tracer is specific for tumor detection.[57]

### b)$^{1}$H MRSI

has been applied in parallel with anatomic MRI for evaluating biochemical changes associated with neoplasia, mainly applied to the diagnosis, preoperative evaluation, and post-treatment monitoring of brain, breast and prostate cancer.[58] $^{1}$H MRSI is most commonly used for the clinical evaluation of brain tumors, and may be helpful in staging glial neoplasms. Brain tumors include a variety of subtypes with a wide range of histopathology, phenotypes and therefore a variety of treatment possibilities.[59] Lactate or lipid presence in the tumor lesions can be considered a hallmark of tumor aggressiveness and therefore may aid in glioma grading *in vivo*.[60] Because of their high proliferation rate, Cho is another biochemical marker used to evaluate the aggressiveness of gliomas, with a higher concentration found in tumors than in normal brain tissue. Together with Cho analysis, quantification of NAA is performed to evaluate neuronal death induced by the tumor.[61, 62] Cho and NAA quantification using $^{1}$H MRSI is particularly useful for radiation treatment follow-up because it is able to distinguish recurrent tumor from radiation necrosis. In both cases, NAA is decreased because of the neuronal loss, but it is possible to see the efficacy of the radiation in the tumor region by a strong decrease of Cho (proliferation marker).[63] Cho measurements are also used for the characterization of breast cancer and its response to chemotherapy. Chen et al. published a recent article describing the clinical evaluation of neoadjuvant chemotherapy (NAC) using MRI for breast cancer. MRSI is able to detect early changes in lipids metabolism. The authors suggest that performing diffusion weighted imaging (DWI), dynamic contrast-enhanced MRI (DCE-MRI) together with MRSI will generate a more complete evaluation of treatment response. Therefore, multi-parametric MRI is proposed as a new tool to evaluate NAC treatment response.[64]

MSRI is a very powerful tool to identify prostate cancer. Cho and citrate are important metabolites evaluated in prostate cancer to assess cell proliferation and prostate gland secretory function. Citrate is abundant in healthy glandular tissues, and its production and secretion is drastically reduced in prostate cancer due to changes in zinc transporter activity.[65, 66]

### c) $^{13}$C MRSI and HP MRI

In the setting of cancer metabolic imaging, $^{13}$C MRSI at thermal equilibrium has limited application due to its low sensitivity in comparison to $^{1}$H MRSI.[67] Thus, with the introduction of HP MRI techniques, altered metabolism in cancer has evolved as a major target. HP [1-$^{13}$C] pyruvate is the most widely used molecule in HP MRI. It is taken up from the blood stream and transported into cells via monocarboxylate transporters (MCTs) and subsequently converted into lactate by lactate dehydrogenase (LDH) with NADH as a cofactor. Cancer cells harboring deregulated glycolytic metabolism therefore show increased lactate production, relative to benign tissues. This phenotype has been successfully demonstrated in a wide range of cancers including prostate, breast, metastatic renal carcinoma, gliomas and lymphoma. Moreover, HP pyruvate has been used to not only

differentiate metabolic rates between tumor and surrounding healthy tissues, but also metabolic differences within the tumor correlating with the heterogeneity of the tumor lesion.[68-70] In addition to pyruvate, many other HP probes have been developed and used to study metabolic pathways in cancer, including HP [1-$^{13}$C] Vitamin C and [1-$^{13}$C] dehydroascorbic acid to measure the redox status of cancer cells, [5-$^{13}$C] glutamine to for glutaminolysis and [$^{13}$C] bicarbonate to measure the acidic tumoral microenvironment.[71-74]

## 3. Brain metabolism imaging

The central nervous system (CNS) is the most metabolic active organ in the human body. The main source of energy for the brain is the oxidation of glucose, where it consumes 20% of the total glucose derived energy from the body, and most of this energy is then used in synaptic activity. Under resting conditions, all of the brain regions are metabolically active with a cerebral metabolic rate for glucose (CMRGlc) of 56 mg per kg of brain tissue, at a ratio of 4.1:1 of oxygen to glucose consumption. The total glucose consumption is strongly upregulated during functional brain activation (0.4:1) indicating preferential increased glycolysis and vice versa down-regulation when function is depressed.[75] Local rates of glucose consumption in different brain compartments are determined by functional and energetic needs. Because glucose is the main source of energy for the brain, [$^{18}$F]FDG has been used to determine different transport rates from blood to the brain by a carrier-mediated diffusion mechanism. In the brain, it is promptly metabolized *via* the glycolytic pathway (described above).[76] [$^{18}$F]FDG pharmacokinetic modeling using Patlak analysis, with an arterial or image-derived input function, is the most widely accepted clinical PET tool to quantitatively estimate the CMRGlc.[77]

Magnetic resonance techniques have also been explored to study brain metabolism. $^{13}$C MRSI performed after infusion of [1-$^{13}$C] glucose and [1-$^{13}$C] acetate has been used to determine hyper-metabolism or hypo-metabolism with varying brain pathologies.[78, 79] For example, these methods can provide information about metabolic alterations in hepatic encephalopathy, demonstrating altered brain glucose oxidation with an impaired metabolism to glutamate. [1-$^{13}$C] acetate can be used to evaluate TCA cycle rate and glutamate and glutamine cycling in patients affected by epilepsy who are glucose intolerant.[79] In addition, MRI using hyperpolarized xenon ($^{129}$Xe) has been used to evaluate the brain activation in normal rats after pain stimuli. The $^{129}$Xe distribution is co-localized with the activation pattern of the rat brain and determined by conventional blood oxygenation level dependent imaging (BOLD) MRI.[80]

### a) Neurodegenerative diseases

Are pathological conditions affecting neurons, the functional units of the brain. The classification of these diseases depend of their etiology, pathophysiology and anatomical localization.[81] Neurodegenerative diseases are progressive pathologies with a poor prognosis, and typically with a complex onset overlapping other pathologies rendering them very difficult to diagnose.[82] With that in mind, metabolic imaging has been utilized extensively to try and aid in the characterization of these disorders, demonstrating the wide potential of variability in this group of diseases.

Alzheimer disease (AD) is characterized microscopically by a deposition of plaque in neurofibrillary tangles, loss of synaptic connections, loss of neurons and hypometabolism.[83] The incidence rate of AD among people 65+ years of age is 19.4 and 15.0 per 1000 person-years for Europe and USA, respectively, and increases exponentially with age.[84] AD patients are characterized by a specific [$^{18}$F]FDG hypo-metabolism pattern in the posterior cingulate cortex, temporal-parietal regions and in the frontal lobes.[85, 86] This hypo-metabolism in AD patients can also present in regions of varying amyloid deposition, and not necessarily directly correlated. Klupp et al. performed a longitudinal study in 15 initial diagnoses of mild, probable AD patients using $^{11}$C-Pittsburgh compound B ($^{11}$C-PiB) to image plaque deposition and [$^{18}$F]FDG PET to image FDG metabolism. They found that AD patients present a typical pattern of amyloid deposition and hypometabolism in the prefrontal region. Moreover, they describe a point-to-cause relationship between increase in toxic amyloid and metabolic decrease in the distal brain area due to disturbed neuronal activity and functionality.[87] $^{1}$H MRSI has further shown that AD patients demonstrate a lower level of NAA in comparison to controls. Moreover, the myo-inositol to Cr level increases substantially in Alzheimer affected patients, which is correlated with glial proliferation.[88]

Parkinson's disease (PD) is a slow progression neurodegenerative disorder with a high incidence in elderly people, increasing exponentially with age. The deposition of neuromyelin and loss of dopaminergic neurons in the substantia nigra are the hallmarks of this pathology.[89, 90] There is significant evidence that mitochondrial respiratory chain dysfunction and oxidative stress could play a role in PD pathogenesis.[91] Most of the techniques for imaging Parkinson are based on specific molecular target, rather than metabolism. Hypometabolism mapping of the brain has been performed using [$^{18}$F]FDG, showing a cerebral hypometabolic pattern in the contralateral parieto-occipital and frontal region.[92] In 2014 a study correlated hypometabolism using FDG PET with hypoxic regions using $H_2{}^{15}O$ PET. Studies using $^{1}$H and $^{31}$P MRSI are still under examination because of their contradictory outcomes.[93]

Multiple Sclerosis (MS) is an autoimmune inflammatory disease of the CNS characterized by the activation of microglia with subsequent astrocyte demyelination. This pathology is not typically considered a neurodegenerative disease, because astrocytes are involved directly in the pathogenesis and not neurons, but evidence is mounting which describe the autonomous neurodegenerative process contributing to whole nervous system degeneration in MS.[94] [$^{18}$F]FDG has been used to detect activation of microglia because of the increase metabolic rate of these specialized macrophages. An interesting study published in 2014, described for the first time the use of [$^{11}$C]acetate as a potential diagnostic tools for the MS. In this study, increased uptake of [$^{11}$C]acetate was shown in hypertrophic MS lesions. More PET probes have been synthesized recently, but only those which target specific markers on the activated microglia of myelin, which are outside of the scope of this review. NAA is a marker for mitochondrial and neuronal integrity, lactate, anaerobic metabolism, and in this specific case, they were used simultaneously to evaluate axonal integrity in patients affected by MS.[95, 96] Brain quantification of NAA with $^{1}$H MRSI is widely used to assess MS and, with a significant reduction in NAA-levels in MS, lesions are observed in comparison to normal appearing white matter. [2, 46, 97]

### b) Traumatic Brain Injuries (TBI)

TBI is the most frequent cause of death in people under the age of 45 and is a primary cause of morbidity in developed countries, with a incidence of 250 per 100,000 people in the European Union and around 100 per 100,000 people in the USA.[98, 99] TBI can be represented with the Glasgow Coma Scale, which ranges from mild injuries, where the lesions are reversible with a complete neurological recovery, to severe injuries, where patients present comatose and are unable to follow commands.[100] Hypometabolism after TBI can easily be diagnosed by PET FDG and correlates with the most negative behavioral and cognitive outcomes.[101, 102] $^{1}$H-MRS has been used to evaluate changes in myelination, neuronal density and edema after TBI.[103] Increases in lactate levels has been observed indicating hypoxia/ischemia in focal injuries. Reduced NAA/Cr and NAA/Cho are also observed in patients within the first 24 hours post-injury, indicating neuronal loss and metabolic depression. Elevated Cho and macromolecules are often observed in those patients, further indicating neuronal loss.[104]

Metabolic imaging is currently used in brain diseases, predominantly through glycolysis with FDG PET and $^{1}$H MRSI for NAA and Cho/Cr, but this is an untapped area, which requires further insight and investigation. The main limitation of brain metabolic imaging is the overlapping of various symptoms and metabolic characteristics with different pathologies. A careful analysis of the symptoms and an accurate standardization is required to understand the correlation between the cause and effect of specific brain diseases.

## 4. Cardiac metabolism imaging

Under normoxic conditions, oxidative phosphorylation is the principal pathway involved in producing energy. In a normal heart, the major source of ATP is fatty acids, which is preferable over carbohydrate sources. According to Randle cycle, in the presence of both substrates, between 60 to 90% of oxygen is consumed to oxidize fatty acids.[105] Both substrates are absorbed to the cytosol trough specific transporters and, after internalization, are metabolized and these metabolic intermediates are transported into the inner mitochondrial membrane to supply the Krebs cycle for the production of NADH, $FADH_2$ and GTP. These reducing equivalents are then used by the electron transport chain for the production of ATP.[106, 107] During ischemia, reversible metabolic adaptations will occur to survive hypo-oxygenation due to the lack of oxygen supply in blood. Mitochondrial oxidation is suppressed and anaerobic metabolism can proceed. If this metabolic shift is impaired, first a contractile dysfunction will occur leading to cell death and, finally, tissues necrosis.

Several PET tracers have been used to image the qualitative and semi-quantitatively metabolic pathways involved in heart metabolism. For free fatty acid metabolic imaging, [$^{11}$C]palmitate has been produced and used to follow beta-oxidation.[108, 109] This tracer is taken up into active cells and undergoes beta-oxidation, leading the production of $^{11}CO_2$. In 1977, E. Weiss et al. demonstrated for the first time, that [$^{11}$C]palmitate could visualize qualitative heart infarction by diminished uptake of the radiotracer in ischemic injuries. Moreover, they have demonstrated that it is not just a matter of limited perfusion of the infarcted area, but that the decrease correlates with a low level of CPK and necrosiss.[108, 109]

Indeed, [$^{11}$C]palmitate is widely used in cardiologic imaging. One of its limitations is the accessibility for imaging centers without cyclotrons due to its short half life (20 min), therefore other radiopharmaceutical analogues using long half-life isotopes have been synthesized including, [$^{123}$I] BMIPP.

Clearance rates of [$^{11}$C] acetate have been widely used to assess myocardial oxygen consumption (MVO2). Amino acid metabolism in the ischemic heart has also been evaluated. Branched-chain amino acid (BCAA) catabolism appears to be upregulated in cardiac tissues. BCAAs are essential for protein synthesis, energy homeostasis and signaling pathways. The catabolic products of these amino acids are acetyl-CoA and succinyl-CoA, which are consumed through direction into the TCA cycle for NADH production.[110] However, during pathological conditions, such as heart failure, myocardial cells suffer from energy starvation, leading to metabolic adaptations, such as increased catabolism of AAs to replenish the energy balance needed for cell survival.[111, 112] Aside from $^{11}$C acetate, two other radiolabeled amino acids have been used to evaluate cardiac conditions, [$^{13}$N] glutamate and [$^{11}$C] methionine. In both cases, investigators reported increased radiopharmaceutical accumulation in the infarcted areas, while retention of the perfusion tracers, [$^{13}$N] ammonia or $^{201}$Thallium, remained unchanged.[113, 114]

Cardiac magnetic resonance (CMR) is a well-established technique used as a routine clinical practice to investigate cardiac function and viability.[115] Myocardial lipids and total Cr are two important markers evaluated in CMR in order to understand healthy or pathological cardiac metabolism.[115] $^{31}$P magnetic resonance spectroscopy ($^{31}$P MRS) is another technique widely used in cardiac imaging to evaluate the phosphocreatine (PCr) to adenosine triphosphate (ATP) ratio, providing an index of the energetic state of the heart.[116-118] In patients with heart failure due to impaired cardiac metabolism, the PCr/ATP level is significantly decreased. This alteration correlates with the degree of heart failure and potentially predicts mortality in patients with dilated cardiomyophaty.[119, 120]

*In vivo* $^{13}$C MRI studies at thermodynamic equilibrium have been limited in animal models due the low sensitivity of MRS. Most studies have been performed after infusion of $^{13}$C enriched molecules using very long scan times, and thus, limited to the study of steady-state metabolite concentrations.[121, 122] To overcome this low sensitivity, preliminary studies in animal models have been performed to evaluate the feasibility of HP MRI for cardiac metabolic imaging.[122] HP [1-$^{13}$C] pyruvate was used in perfused rodent hearts to assess PDH flux by quantifying its metabolite, $^{13}$C bicarbonate. PDH is an essential regulatory enzyme of the Randle cycle (described above).[123, 124] Recent work in a porcine ischemic heart model has further demonstrated the feasibility of HP [1-$^{13}$C] pyruvate to distinguish early metabolic changes found within intact cells during ischemia. Lactate, alanine and bicarbonate maps may provide information about the metabolic status and viability of ischemic myocardium.[125]

Currently, MRS is the most promising technique able to supply information about metabolism and pathophysiology of many cardiac conditions. MRS provides insight into cardiac metabolism and, in particular, energetics of the cardiac tissue in normal and disease states without exposing the patient to ionizing radiation. The future of cardiac metabolic

imaging relies on technology development, such as increases in magnetic field strength for MRI scanners. This will provide increased signal for stable $^{13}C$ molecules and respective metabolites. Nonetheless, HP MRI may represent a novel technique in this regard, that may combine with the use of 3T and lower MRI scanner since the signal-to-noise ratio derived from the $^{13}C$-labeled metabolites is already increased several orders of magnitude. Moreover, using lower magnetic fields may be possible to prolong the relaxation time of the $^{13}C$ molecules and therefore follow their metabolism for longer timeframes.

## 5. Inflammation/Infection

The inflammatory cascade begins when pathogen associate molecular patterns (PAMPs) or damage-associate molecular patterns (DAMPs), derived from the host pathogen or injured tissue, are recognized by the host immune system.[126] Upon ligand recognition, a phenotypic switch is activated in immune cells. After activation, depending on immune cell lineage, metabolism changes drastically. Under normal conditions, resting myeloid cells use glycolysis to generate energy, whereas resting lymphocytes use oxidative phosphorylation of amino acids, glucose and lipids.[127] After activation a metabolic shift is observed where T- and B-lymphocytes rely on aerobic glycolysis along with glutamine oxidation. A 40-fold increase in lactate production is observed in mitogen stimulated T cells, making it similar to the metabolic shift observed in transformed cancer cells (Warburg effect).[128]

Inflammation is accompanied not only by immune cell infiltration but also by increased blood supply, vascular permeability and augmented protein transudation in the inflammatory foci.[129, 130] Because of these changes, several molecules have been used to follow changes in the microenvironment. Scintigraphic detection of inflammation using non-specific tracers such as $^{67}$Gallium citrate, labeled non-specific immunoglobulins and liposomes has been tested in different pathologies. The main limitation is the high background uptake due to high permeability in well-perfused organs. To date, direct and indirect labeling of immunes cells such as [$^{99m}$Tc] HMPAO labeled leucocytes are the gold standard for evaluating inflammation though these are not metabolic probes.[130-134] [$^{18}$F]FDG is the only radiopharmaceutical used to target metabolic changes in the immune cells for the assessment of inflammatory processes. An extensive review published on 2013 by Glaudemans et al describes in depth the advantages and disadvantages of this technique in various clinical cases. For diagnosis, a low dose CT scan follows the FDG PET scan in order to evaluate structural alterations, such as calcification, thrombosis and wall thickening. The information derived from metabolic imaging using FDG and the anatomical information gathered from CT is taken into account, although lack of specificity may make clinical decision-making difficult.[135-139]

Recent strategies targeting bacterial metabolism suggest that the metabolic imaging of infection may soon be integrated into routine clinical practice, to assess both sites of infection and proper response to antibiotic therapy. One limitation of using $^{18}$F-FDG to image infection is that it targets host response rather than features of living bacteria, and thus cannot distinguish infection from sterile inflammation. One recent approach used $^{18}$F-fluorodeoxysorbitol (FDS), which was originally considered for tumor imaging but shows much more promise in imaging Gram (-) bacteria.[140] Other reported methods use either $^{18}$F

labeled versions of maltose and maltohexose, potentially targeting both Gram (-) and Gram (+) bacteria. $^{18}$F maltose is radiolabeled via a simple synthesis similar to that of $^{18}$F-FDG, but may suffer from stability issues due to mammalian metabolism of the α 1,4 glycolytic linkage. Results in animal models suggest that $^{18}$F maltohexose may be more stable *in vivo*.[141] Metabolic approaches to image bacterial infections are particularly attractive in the context of increased interest in full-body metabolic scanning via PET-CT or more recently PET-MR.

## 6. Conclusions

FDG PET is the most common metabolic imaging method, used to assess hypo and hyper metabolism in various clinical conditions. It is widely used in routine clinical practice; however, future improvements are urgently needed to address its specificity. Magnetic resonance spectroscopy imaging allows detection and resolution of metabolites of interest utilizing their molecular structure, though it suffers from sensitivity *in vivo*. The development of hyperpolarized MRI as a new diagnostic platform has the potential to image metabolism in real time. $^{13}$C pyruvate using hyperpolarized MRI has been most utilized in cancer metabolism imaging, however applications in different pathological conditions, such as cardiac imaging have been proven successful. In the future, new probes for both PET and hyperpolarized MRI will provide researchers and clinicians with an arsenal of tools to better study metabolism. Moreover, hybrid imaging has the potential to combine sensitivity and specificity of these different imaging methodologies to create the ideal approach to assess metabolism in humans.

## Acknowledgments

Funding for this is through the National institute of health NIH R00 EB014328 (KRK) and R01 CA166766 (DMW). VD, DMW and KRK conceived of the review and were responsible for its writing. The authors declare no conflict of interest.

## References

1. Rao NP, Venkatasubramanian G, Gangadhar BN. Proton magnetic resonance spectroscopy in depression. Indian J Psychiatry. 2011; 53:307–11. [PubMed: 22303038]
2. Castillo M, Kwock L, Mukherji SK. Clinical applications of proton MR spectroscopy. AJNR Am J Neuroradiol. 1996; 17:1–15. [PubMed: 8770242]
3. Sailasuta N, et al. Clinical NOE 13C MRS for neuropsychiatric disorders of the frontal lobe. J Magn Reson. 2008; 195:219–25. [PubMed: 18829354]
4. Shic F, Ross B. Automated data processing of [1H-decoupled] 13C MR spectra acquired from human brain in vivo. J Magn Reson. 2003; 162:259–68. [PubMed: 12810010]
5. Gruetter R, Adriany G, Merkle H, Andersen PM. Broadband decoupled, 1H-localized 13C MRS of the human brain at 4 Tesla. Magn Reson Med. 1996; 36:659–64. [PubMed: 8916015]
6. Kurhanewicz J, Bok R, Nelson SJ, Vigneron DB. Current and potential applications of clinical 13C MR spectroscopy. J Nucl Med. 2008; 49:341–4. [PubMed: 18322118]
7. Befroy DE, Shulman GI. Magnetic resonance spectroscopy studies of human metabolism. Diabetes. 2011; 60:1361–9. [PubMed: 21525507]
8. Gallagher FA, et al. Hyperpolarized 13C MRI and PET: in vivo tumor biochemistry. J Nucl Med. 2011; 52:1333–6. [PubMed: 21849405]
9. Keshari KR, Wilson DM. Chemistry and biochemistry of 13C hyperpolarized magnetic resonance using dynamic nuclear polarization. Chem Soc Rev. 2014; 43:1627–59. [PubMed: 24363044]

10. Lu J, Tan M, Cai Q. The Warburg effect in tumor progression: mitochondrial oxidative metabolism as an anti-metastasis mechanism. Cancer Lett. 2015; 356:156–64. [PubMed: 24732809]
11. Moraes TF, Reithmeier RA. Membrane transport metabolons. Biochim Biophys Acta. 2012; 1818:2687–706. [PubMed: 22705263]
12. Thorens B, Mueckler M. Glucose transporters in the 21st Century. Am J Physiol Endocrinol Metab. 2010; 298:E141–5. [PubMed: 20009031]
13. Cox BL, Mackie TR, Eliceiri KW. The sweet spot: FDG and other 2-carbon glucose analogs for multi-modal metabolic imaging of tumor metabolism. Am J Nucl Med Mol Imaging. 2015; 5:1–13. [PubMed: 25625022]
14. Kamphorst JJ, Chung MK, Fan J, Rabinowitz JD. Quantitative analysis of acetyl-CoA production in hypoxic cancer cells reveals substantial contribution from acetate. Cancer Metab. 2014; 2:23. [PubMed: 25671109]
15. Alderton GK. Metabolism: acetate nourishes stressed tumour cells. Nat Rev Cancer. 2015; 15:67. [PubMed: 25613999]
16. Grassi I, et al. The clinical use of PET with (11)C-acetate. Am J Nucl Med Mol Imaging. 2012; 2:33–47. [PubMed: 23133801]
17. de Graaf RA, Rothman DL, Behar KL. State of the art direct 13C and indirect 1H-[13C] NMR spectroscopy in vivo. A practical guide. NMR Biomed. 2011; 24:958–72. [PubMed: 21919099]
18. Mishkovsky M, Comment A, Gruetter R. In vivo detection of brain Krebs cycle intermediate by hyperpolarized magnetic resonance. J Cereb Blood Flow Metab. 2012; 32:2108–13. [PubMed: 22990416]
19. Schroeder MA, et al. Real-time assessment of Krebs cycle metabolism using hyperpolarized 13C magnetic resonance spectroscopy. FASEB J. 2009; 23:2529–38. [PubMed: 19329759]
20. Koellisch U, et al. Metabolic imaging of hyperpolarized [1- C]acetate and [1- C]acetylcarnitine - investigation of the influence of dobutamine induced stress. Magn Reson Med. 2014
21. Bastiaansen JA, et al. In vivo enzymatic activity of acetylCoA synthetase in skeletal muscle revealed by (13)C turnover from hyperpolarized [1-(13)C]acetate to [1-(13)C]acetylcarnitine. Biochim Biophys Acta. 2013; 1830:4171–8. [PubMed: 23545238]
22. Josan S, et al. Dynamic metabolic imaging of hyperpolarized [2-(13) C]pyruvate using spiral chemical shift imaging with alternating spectral band excitation. Magn Reson Med. 2014; 71:2051–8. [PubMed: 23878057]
23. Corbin KD, Zeisel SH. Choline metabolism provides novel insights into nonalcoholic fatty liver disease and its progression. Curr Opin Gastroenterol. 2012; 28:159–65. [PubMed: 22134222]
24. Glunde K, Bhujwalla ZM, Ronen SM. Choline metabolism in malignant transformation. Nat Rev Cancer. 2011; 11:835–48. [PubMed: 22089420]
25. Aboagye EO, Bhujwalla ZM. Malignant transformation alters membrane choline phospholipid metabolism of human mammary epithelial cells. Cancer Res. 1999; 59:80–4. [PubMed: 9892190]
26. Wyss M, Kaddurah-Daouk R. Creatine and creatinine metabolism. Physiol Rev. 2000; 80:1107–213. [PubMed: 10893433]
27. Brosnan JT, Brosnan ME. Creatine metabolism and the urea cycle. Mol Genet Metab. 2010; 100 Suppl 1:S49–52. [PubMed: 20304692]
28. Wackerhage H, et al. Glycolytic ATP production estimated from 31P magnetic resonance spectroscopy measurements during ischemic exercise in vivo. MAGMA. 1996; 4:151–5. [PubMed: 9220403]
29. Rajagopalan B, Blackledge MJ, McKenna WJ, Bolas N, Radda GK. Measurement of phosphocreatine to ATP ratio in normal and diseased human heart by 31P magnetic resonance spectroscopy using the rotating frame-depth selection technique. Ann N Y Acad Sci. 1987; 508:321–32. [PubMed: 3439707]
30. Newsholme P, Procopio J, Lima MM, Pithon-Curi TC, Curi R. Glutamine and glutamate--their central role in cell metabolism and function. Cell Biochem Funct. 2003; 21:1–9. [PubMed: 12579515]
31. Newsholme P, et al. Glutamine and glutamate as vital metabolites. Braz J Med Biol Res. 2003; 36:153–63. [PubMed: 12563517]

32. Qu W, et al. Preparation and characterization of L-[5-11C]-glutamine for metabolic imaging of tumors. J Nucl Med. 2012; 53:98–105. [PubMed: 22173839]
33. Qu W, et al. Synthesis of optically pure 4-fluoro-glutamines as potential metabolic imaging agents for tumors. J Am Chem Soc. 2011; 133:1122–33. [PubMed: 21190335]
34. Qu W, et al. Facile synthesis [5-(13)C-4-(2)H(2)]-L-glutamine for hyperpolarized MRS imaging of cancer cell metabolism. Acad Radiol. 2011; 18:932–9. [PubMed: 21658976]
35. Wu Z, et al. [(18)F](2S,4S)-4-(3-Fluoropropyl)glutamine as a tumor imaging agent. Mol Pharm. 2014; 11:3852–66. [PubMed: 25095908]
36. Gallagher FA, Kettunen MI, Day SE, Lerche M, Brindle KM. 13C MR spectroscopy measurements of glutaminase activity in human hepatocellular carcinoma cells using hyperpolarized 13C-labeled glutamine. Magn Reson Med. 2008; 60:253–7. [PubMed: 18666104]
37. Wilson DM, Kurhanewicz J. Hyperpolarized 13C MR for molecular imaging of prostate cancer. J Nucl Med. 2014; 55:1567–72. [PubMed: 25168625]
38. Rothman DL, De Feyter HM, de Graaf RA, Mason GF, Behar KL. 13C MRS studies of neuroenergetics and neurotransmitter cycling in humans. NMR Biomed. 2011; 24:943–57. [PubMed: 21882281]
39. Canape C, et al. Probing treatment response of glutaminolytic prostate cancer cells to natural drugs with hyperpolarized [5- C]glutamine. Magn Reson Med. 2015; 73:2296–2305. [PubMed: 25045880]
40. Locasale JW. Serine, glycine and one-carbon units: cancer metabolism in full circle. Nat Rev Cancer. 2013; 13:572–83. [PubMed: 23822983]
41. Langstrom B, et al. Synthesis of L- and D-[methyl-11C]methionine. J Nucl Med. 1987; 28:1037–40. [PubMed: 3585494]
42. Bergstrom M, et al. Comparison of the accumulation kinetics of L-(methyl-11C)-methionine and D-(methyl-11C)-methionine in brain tumors studied with positron emission tomography. Acta Radiol. 1987; 28:225–9. [PubMed: 2958026]
43. Siegel RL, Miller KD, Jemal A. Cancer statistics, 2015. CA Cancer J Clin. 2015; 65:5–29. [PubMed: 25559415]
44. Cairns RA, Harris I, McCracken S, Mak TW. Cancer cell metabolism. Cold Spring Harb Symp Quant Biol. 2011; 76:299–311. [PubMed: 22156302]
45. Warburg O. On the origin of cancer cells. Science. 1956; 123:309–14. [PubMed: 13298683]
46. Aboul-Enein F, Krssak M, Hoftberger R, Prayer D, Kristoferitsch W. Reduced NAA-levels in the NAWM of patients with MS is a feature of progression. A study with quantitative magnetic resonance spectroscopy at 3 Tesla. PLoS One. 2010; 5:e11625. [PubMed: 20652023]
47. Kim JW, Dang CV. Cancer's molecular sweet tooth and the Warburg effect. Cancer Res. 2006; 66:8927–30. [PubMed: 16982728]
48. DeBerardinis RJ, et al. Beyond aerobic glycolysis: transformed cells can engage in glutamine metabolism that exceeds the requirement for protein and nucleotide synthesis. Proc Natl Acad Sci U S A. 2007; 104:19345–50. [PubMed: 18032601]
49. Cantor JR, Sabatini DM. Cancer cell metabolism: one hallmark, many faces. Cancer Discov. 2012; 2:881–98. [PubMed: 23009760]
50. Cairns RA, Harris IS, Mak TW. Regulation of cancer cell metabolism. Nat Rev Cancer. 2011; 11:85–95. [PubMed: 21258394]
51. Zhu A, Lee D, Shim H. Metabolic positron emission tomography imaging in cancer detection and therapy response. Semin Oncol. 2011; 38:55–69. [PubMed: 21362516]
52. Plathow C, Weber WA. Tumor cell metabolism imaging. J Nucl Med. 2008; 49 Suppl 2:43S–63S. [PubMed: 18523065]
53. Weber WA, Schwaiger M, Avril N. Quantitative assessment of tumor metabolism using FDG-PET imaging. Nucl Med Biol. 2000; 27:683–7. [PubMed: 11091112]
54. Almuhaideb A, Papathanasiou N, Bomanji J. 18F-FDG PET/CT imaging in oncology. Ann Saudi Med. 2011; 31:3–13. [PubMed: 21245592]
55. Schwarzenbock S, Souvatzoglou M, Krause BJ. Choline PET and PET/CT in Primary Diagnosis and Staging of Prostate Cancer. Theranostics. 2012; 2:318–30. [PubMed: 22448198]

56. Kameyama M, et al. The accumulation of 11C-methionine in cerebral glioma patients studied with PET. Acta Neurochir (Wien). 1990; 104:8–12. [PubMed: 2386094]
57. Venneti S, et al. Glutamine-based PET imaging facilitates enhanced metabolic evaluation of gliomas in vivo. Sci Transl Med. 2015; 7:274ra17.
58. Pinker K, Stadlbauer A, Bogner W, Gruber S, Helbich TH. Molecular imaging of cancer: MR spectroscopy and beyond. Eur J Radiol. 2012; 81:566–77. [PubMed: 20554145]
59. Cha S. Neuroimaging in neuro-oncology. Neurotherapeutics. 2009; 6:465–77. [PubMed: 19560737]
60. Li X, Lu Y, Pirzkall A, McKnight T, Nelson SJ. Analysis of the spatial characteristics of metabolic abnormalities in newly diagnosed glioma patients. J Magn Reson Imaging. 2002; 16:229–37. [PubMed: 12205577]
61. Negendank WG, et al. Proton magnetic resonance spectroscopy in patients with glial tumors: a multicenter study. J Neurosurg. 1996; 84:449–58. [PubMed: 8609557]
62. Hourani R, et al. Proton magnetic resonance spectroscopic imaging to differentiate between nonneoplastic lesions and brain tumors in children. J Magn Reson Imaging. 2006; 23:99–107. [PubMed: 16374884]
63. Fan G. Comments and controversies: magnetic resonance spectroscopy and gliomas. Cancer Imaging. 2006; 6:113–5. [PubMed: 16966066]
64. Chen JH, Su MY. Clinical application of magnetic resonance imaging in management of breast cancer patients receiving neoadjuvant chemotherapy. Biomed Res Int. 2013; 2013:348167. [PubMed: 23862143]
65. Kurhanewicz J, Vigneron DB. Advances in MR spectroscopy of the prostate. Magn Reson Imaging Clin N Am. 2008; 16:697–710. ix–x. [PubMed: 18926432]
66. Li B, et al. Magnetic resonance imaging for prostate cancer clinical application. Chin J Cancer Res. 2013; 25:240–9. [PubMed: 23592906]
67. Li Y, Park I, Nelson SJ. Imaging tumor metabolism using in vivo magnetic resonance spectroscopy. Cancer J. 2015; 21:123–8. [PubMed: 25815853]
68. Albers MJ, et al. Hyperpolarized 13C lactate, pyruvate, and alanine: noninvasive biomarkers for prostate cancer detection and grading. Cancer Res. 2008; 68:8607–15. [PubMed: 18922937]
69. Lupo JM, et al. Analysis of hyperpolarized dynamic 13C lactate imaging in a transgenic mouse model of prostate cancer. Magn Reson Imaging. 2010; 28:153–62. [PubMed: 19695815]
70. Keshari KR, et al. Hyperpolarized 13C-pyruvate magnetic resonance reveals rapid lactate export in metastatic renal cell carcinomas. Cancer Res. 2013; 73:529–38. [PubMed: 23204238]
71. Bohndiek SE, et al. Hyperpolarized [1-13C]-ascorbic and dehydroascorbic acid: vitamin C as a probe for imaging redox status in vivo. J Am Chem Soc. 2011; 133:11795–801. [PubMed: 21692446]
72. Keshari KR, et al. Hyperpolarized [1-13C]dehydroascorbate MR spectroscopy in a murine model of prostate cancer: comparison with 18F-FDG PET. J Nucl Med. 2013; 54:922–8. [PubMed: 23575993]
73. Gallagher FA, Kettunen MI, Brindle KM. Imaging pH with hyperpolarized 13C. NMR Biomed. 2011; 24:1006–15. [PubMed: 21812047]
74. Gallagher FA, et al. Magnetic resonance imaging of pH in vivo using hyperpolarized 13C-labelled bicarbonate. Nature. 2008; 453:940–3. [PubMed: 18509335]
75. Mergenthaler P, Lindauer U, Dienel GA, Meisel A. Sugar for the brain: the role of glucose in physiological and pathological brain function. Trends Neurosci. 2013; 36:587–97. [PubMed: 23968694]
76. Hasselbalch SG, et al. Transport of D-glucose and 2-fluorodeoxyglucose across the blood-brain barrier in humans. J Cereb Blood Flow Metab. 1996; 16:659–66. [PubMed: 8964806]
77. Chen K, et al. Noninvasive quantification of the cerebral metabolic rate for glucose using positron emission tomography, 18F-fluoro-2-deoxyglucose, the Patlak method, and an image-derived input function. J Cereb Blood Flow Metab. 1998; 18:716–23. [PubMed: 9663501]
78. Gruetter R, et al. Direct measurement of brain glucose concentrations in humans by 13C NMR spectroscopy. Proc Natl Acad Sci U S A. 1992; 89:1109–12. [PubMed: 1736294]

79. Ross B, Lin A, Harris K, Bhattacharya P, Schweinsburg B. Clinical experience with 13C MRS in vivo. NMR Biomed. 2003; 16:358–69. [PubMed: 14679500]
80. Mazzanti ML, et al. Distribution of hyperpolarized xenon in the brain following sensory stimulation: preliminary MRI findings. PLoS One. 2011; 6:e21607. [PubMed: 21789173]
81. Przedborski S, Vila M, Jackson-Lewis V. Neurodegeneration: what is it and where are we? J Clin Invest. 2003; 111:3–10. [PubMed: 12511579]
82. Nasrallah IM, Wolk DA. Multimodality imaging of Alzheimer disease and other neurodegenerative dementias. J Nucl Med. 2014; 55:2003–11. [PubMed: 25413136]
83. Kalia M, Costa ESJ. Biomarkers of psychiatric diseases: current status and future prospects. Metabolism. 2015; 64:S11–5. [PubMed: 25467847]
84. Qiu C, Kivipelto M, von Strauss E. Epidemiology of Alzheimer's disease: occurrence, determinants, and strategies toward intervention. Dialogues Clin Neurosci. 2009; 11:111–28. [PubMed: 19585947]
85. Shokouhi S, Claassen D, Riddle W. Imaging Brain Metabolism and Pathology in Alzheimer's Disease with Positron Emission Tomography. J Alzheimers Dis Parkinsonism. 2014; 4
86. Shivamurthy VK, Tahari AK, Marcus C, Subramaniam RM. Brain FDG PET and the diagnosis of dementia. AJR Am J Roentgenol. 2015; 204:W76–85. [PubMed: 25539279]
87. Klupp E, et al. Prefrontal hypometabolism in Alzheimer disease is related to longitudinal amyloid accumulation in remote brain regions. J Nucl Med. 2015; 56:399–404. [PubMed: 25678488]
88. Graff-Radford J, Kantarci K. Magnetic resonance spectroscopy in Alzheimer's disease. Neuropsychiatr Dis Treat. 2013; 9:687–96. [PubMed: 23696705]
89. Rodriguez M, Rodriguez-Sabate C, Morales I, Sanchez A, Sabate M. Parkinson's disease as a result of aging. Aging Cell. 2015
90. Campos PB, Paulsen BS, Rehen SK. Accelerating neuronal aging in in vitro model brain disorders: a focus on reactive oxygen species. Front Aging Neurosci. 2014; 6:292. [PubMed: 25386139]
91. Groger A, Kolb R, Schafer R, Klose U. Dopamine reduction in the substantia nigra of Parkinson's disease patients confirmed by in vivo magnetic resonance spectroscopic imaging. PLoS One. 2014; 9:e84081. [PubMed: 24416192]
92. Teune LK, et al. Typical cerebral metabolic patterns in neurodegenerative brain diseases. Mov Disord. 2010; 25:2395–404. [PubMed: 20669302]
93. Weiduschat N, et al. Usefulness of proton and phosphorus MR spectroscopic imaging for early diagnosis of Parkinson's disease. J Neuroimaging. 2015; 25:105–10. [PubMed: 24325203]
94. Stadelmann C. Multiple sclerosis as a neurodegenerative disease: pathology, mechanisms and therapeutic implications. Curr Opin Neurol. 2011; 24:224–9. [PubMed: 21455066]
95. Pan JW, Krupp LB, Elkins LE, Coyle PK. Cognitive dysfunction lateralizes with NAA in multiple sclerosis. Appl Neuropsychol. 2001; 8:155–60. [PubMed: 11686650]
96. Narayana PA. Magnetic resonance spectroscopy in the monitoring of multiple sclerosis. J Neuroimaging. 2005; 15:46S–57S. [PubMed: 16385018]
97. Davie CA, et al. Serial proton magnetic resonance spectroscopy in acute multiple sclerosis lesions. Brain. 1994; 117 (Pt 1):49–58. [PubMed: 8149214]
98. Bruns J Jr, Hauser WA. The epidemiology of traumatic brain injury: a review. Epilepsia. 2003; 44 Suppl 10:2–10. [PubMed: 14511388]
99. Roozenbeek B, Maas AI, Menon DK. Changing patterns in the epidemiology of traumatic brain injury. Nat Rev Neurol. 2013; 9:231–6. [PubMed: 23443846]
100. Ghajar J. Traumatic brain injury. Lancet. 2000; 356:923–9. [PubMed: 11036909]
101. Byrnes KR, et al. FDG-PET imaging in mild traumatic brain injury: a critical review. Front Neuroenergetics. 2014; 5:13. [PubMed: 24409143]
102. Nakashima T, et al. Focal brain glucose hypometabolism in patients with neuropsychologic deficits after diffuse axonal injury. AJNR Am J Neuroradiol. 2007; 28:236–42. [PubMed: 17296986]
103. Brenner LA. Neuropsychological and neuroimaging findings in traumatic brain injury and post-traumatic stress disorder. Dialogues Clin Neurosci. 2011; 13:311–23. [PubMed: 22034217]

104. Brooks WM, Friedman SD, Gasparovic C. Magnetic resonance spectroscopy in traumatic brain injury. J Head Trauma Rehabil. 2001; 16:149–64. [PubMed: 11275576]
105. Osterholt M, Sen S, Dilsizian V, Taegtmeyer H. Targeted metabolic imaging to improve the management of heart disease. JACC Cardiovasc Imaging. 2012; 5:214–26. [PubMed: 22340831]
106. Obrzut S, Jamshidi N, Karimi A, Birgersdotter-Green U, Hoh C. Imaging and modeling of myocardial metabolism. J Cardiovasc Transl Res. 2010; 3:384–96. [PubMed: 20559785]
107. Doenst T, Nguyen TD, Abel ED. Cardiac metabolism in heart failure: implications beyond ATP production. Circ Res. 2013; 113:709–24. [PubMed: 23989714]
108. Sobel BE, Weiss ES, Welch MJ, Siegel BA, Ter-Pogossian MM. Detection of remote myocardial infarction in patients with positron emission transaxial tomography and intravenous 11C-palmitate. Circulation. 1977; 55:853–7. [PubMed: 870242]
109. Weiss ES, et al. Quantification of infarction in cross sections of canine myocardium in vivo with positron emission transaxial tomography and 11C-palmitate. Circulation. 1977; 55:66–73. [PubMed: 830220]
110. Huang Y, Zhou M, Sun H, Wang Y. Branched-chain amino acid metabolism in heart disease: an epiphenomenon or a real culprit? Cardiovasc Res. 2011; 90:220–3. [PubMed: 21502372]
111. Marazzi G, Rosanio S, Caminiti G, Dioguardi FS, Mercuro G. The role of amino acids in the modulation of cardiac metabolism during ischemia and heart failure. Curr Pharm Des. 2008; 14:2592–604. [PubMed: 18991676]
112. Barrio JR, et al. Synthesis and myocardial kinetics of N-13 and C-11 labeled branched-chain L-amino acids. J Nucl Med. 1983; 24:937–44. [PubMed: 6619964]
113. Morooka M, et al. 11C-methionine PET of acute myocardial infarction. J Nucl Med. 2009; 50:1283–7. [PubMed: 19617334]
114. Knapp WH, Helus F, Ostertag H, Tillmanns H, Kubler W. Uptake and turnover of L-(13N)-glutamate in the normal human heart and in patients with coronary artery disease. Eur J Nucl Med. 1982; 7:211–5. [PubMed: 6124422]
115. Faller KM, Lygate CA, Neubauer S, Schneider JE. (1)H-MR spectroscopy for analysis of cardiac lipid and creatine metabolism. Heart Fail Rev. 2013; 18:657–68. [PubMed: 22945240]
116. Hudsmith LE, Neubauer S. Magnetic resonance spectroscopy in myocardial disease. JACC Cardiovasc Imaging. 2009; 2:87–96. [PubMed: 19356540]
117. Yabe T, Mitsunami K, Inubushi T, Kinoshita M. Quantitative measurements of cardiac phosphorus metabolites in coronary artery disease by 31P magnetic resonance spectroscopy. Circulation. 1995; 92:15–23. [PubMed: 7788910]
118. Ingwall JS, Weiss RG. Is the failing heart energy starved? On using chemical energy to support cardiac function. Circ Res. 2004; 95:135–45. [PubMed: 15271865]
119. Neubauer S, et al. 31P magnetic resonance spectroscopy in dilated cardiomyopathy and coronary artery disease. Altered cardiac high-energy phosphate metabolism in heart failure. Circulation. 1992; 86:1810–8. [PubMed: 1451253]
120. Neubauer S, et al. Myocardial phosphocreatine-to-ATP ratio is a predictor of mortality in patients with dilated cardiomyopathy. Circulation. 1997; 96:2190–6. [PubMed: 9337189]
121. Ziegler A, Zaugg CE, Buser PT, Seelig J, Kunnecke B. Non-invasive measurements of myocardial carbon metabolism using in vivo 13C NMR spectroscopy. NMR Biomed. 2002; 15:222–34. [PubMed: 11968138]
122. Tyler DJ. Cardiovascular Applications of Hyperpolarized MRI. Curr Cardiovasc Imaging Rep. 2011; 4:108–115. [PubMed: 21475403]
123. Merritt ME, et al. Hyperpolarized 13C allows a direct measure of flux through a single enzyme-catalyzed step by NMR. Proc Natl Acad Sci U S A. 2007; 104:19773–7. [PubMed: 18056642]
124. Schroeder MA, et al. In vivo assessment of pyruvate dehydrogenase flux in the heart using hyperpolarized carbon-13 magnetic resonance. Proc Natl Acad Sci U S A. 2008; 105:12051–6. [PubMed: 18689683]
125. Golman K, et al. Cardiac metabolism measured noninvasively by hyperpolarized 13C MRI. Magn Reson Med. 2008; 59:1005–13. [PubMed: 18429038]

126. Storek KM, Monack DM. Bacterial recognition pathways that lead to inflammasome activation. Immunol Rev. 2015; 265:112–29. [PubMed: 25879288]

127. Kominsky DJ, Campbell EL, Colgan SP. Metabolic shifts in immunity and inflammation. J Immunol. 2010; 184:4062–8. [PubMed: 20368286]

128. MacIver NJ, Michalek RD, Rathmell JC. Metabolic regulation of T lymphocytes. Annu Rev Immunol. 2013; 31:259–83. [PubMed: 23298210]

129. Rennen HJ, Corstens FH, Oyen WJ, Boerman OC. New concepts in infection/inflammation imaging. Q J Nucl Med. 2001; 45:167–73. [PubMed: 11476166]

130. Rennen HJ, Boerman OC, Oyen WJ, Corstens FH. Imaging infection/inflammation in the new millennium. Eur J Nucl Med. 2001; 28:241–52. [PubMed: 11303896]

131. Malviya G, Galli F, Sonni I, Signore A. Imaging T-lymphocytes in inflammatory diseases: a nuclear medicine approach. Q J Nucl Med Mol Imaging. 2014; 58:237–57. [PubMed: 25265246]

132. Agranovich S, Rachinsky I, Pak I, Benkovich E, Lantsberg S. The usefulness of Tc-99m-HMPAO-labeled leukocyte scintigraphy in the diagnosis of multiple intra-abdominal abscesses following in vitro fertilization (IVF) procedure. Eur J Obstet Gynecol Reprod Biol. 2004; 116:103–5. [PubMed: 15294377]

133. Gardner A, et al. 99mTc-HMPAO distribution at SPECT is associated with succinate-cytochrome c reductase (SCR) activity in subjects with psychiatric disorders. Nucl Med Biol. 2004; 31:277–82. [PubMed: 15013494]

134. Pelosi E, et al. 99mTc-HMPAO-leukocyte scintigraphy in patients with symptomatic total hip or knee arthroplasty: improved diagnostic accuracy by means of semiquantitative evaluation. J Nucl Med. 2004; 45:438–44. [PubMed: 15001684]

135. Glaudemans AW, et al. The use of (18)F-FDG-PET/CT for diagnosis and treatment monitoring of inflammatory and infectious diseases. Clin Dev Immunol. 2013; 2013:623036. [PubMed: 24027590]

136. Glaudemans AW, Slart RH, Noordzij W, Dierckx RA, Hazenberg BP. Utility of 18F-FDG PET(/CT) in patients with systemic and localized amyloidosis. Eur J Nucl Med Mol Imaging. 2013; 40:1095–101. [PubMed: 23474745]

137. Love C, Palestro CJ. Radionuclide imaging of inflammation and infection in the acute care setting. Semin Nucl Med. 2013; 43:102–13. [PubMed: 23414826]

138. Basu S, Kumar R, Alavi A. PET and PET-CT imaging in infection and inflammation: its critical role in assessing complications related to therapeutic interventions in patients with cancer. Indian J Cancer. 2010; 47:371–9. [PubMed: 21131748]

139. Saboury B, Torigian DA, Alavi A. Comment on: “FDG PET and PET/CT: EANM procedure guidelines for tumour PET imaging, version 1.0”. Eur J Nucl Med Mol Imaging. 2010; 37:1430–1. author reply 1432-3. [PubMed: 20503048]

140. Weinstein EA, et al. Imaging Enterobacteriaceae infection in vivo with 18F-fluorodeoxysorbitol positron emission tomography. Sci Transl Med. 2014; 6:259ra146.

141. Gowrishankar G, et al. Investigation of 6-[(1)(8)F]-fluoromaltose as a novel PET tracer for imaging bacterial infection. PLoS One. 2014; 9:e107951. [PubMed: 25243851]

142. Choi C, et al. 2-hydroxyglutarate detection by magnetic resonance spectroscopy in IDH-mutated patients with gliomas. Nat Med. 2012; 18:624–9. [PubMed: 22281806]

143. Nelson SJ, et al. Metabolic imaging of patients with prostate cancer using hyperpolarized [1-(1)(3)C]pyruvate. Sci Transl Med. 2013; 5:198ra108.

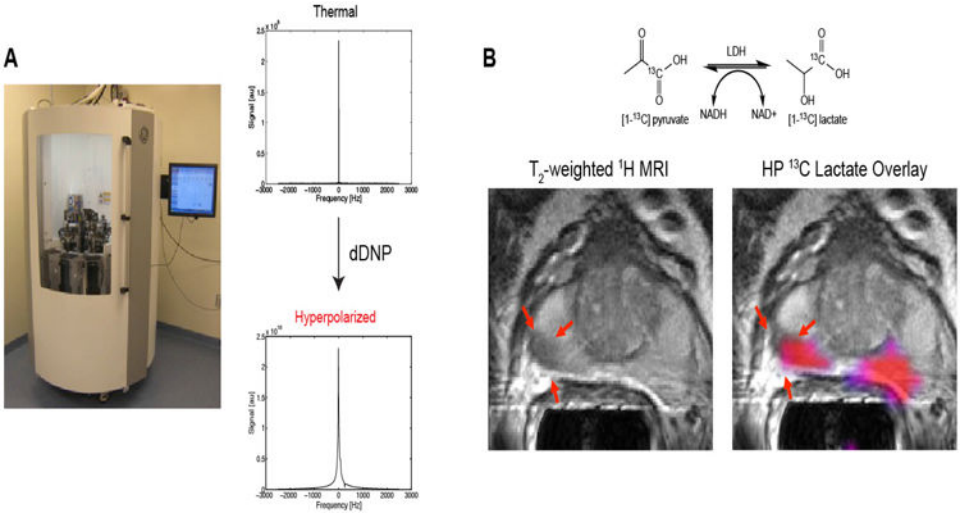


**Figure 1. Spectroscopic imaging of 2HG**

Routine long-echo 1H MRS in brain tumors is frequently used to study glial neoplasms, with associated alterations in choline, creatine, NAA and lactate. In this case, a spectral editing technique was used to uncover the oncometabolite 2HG, which is a biomarker for IDH1 mutant status in low-grade glial neoplasms (**A**) Multivoxel imaging spectra from a subject with a WHO grade 3 oligodendroglioma are overlaid on the $T_2$w-FLAIR image. The grid size is 1 × 1 cm, with slice thickness 1.5 cm. The spectra are displayed between 4.1 ppm and 1.8 ppm (left to right). (**B,C**) Two representative spectra (one from the tumor and another from the contralateral normal brain) are shown together with LCModel fits and residuals. Mins, myoinositol. (**D**) The estimated concentrations of 2HG, choline and NAA in individual voxels were color coded for comparison. The NAA level in gray matter in normal brain was assumed to be 12 mM. Scale bars, 1 cm. *Adapted from C Choi et al.*[142]

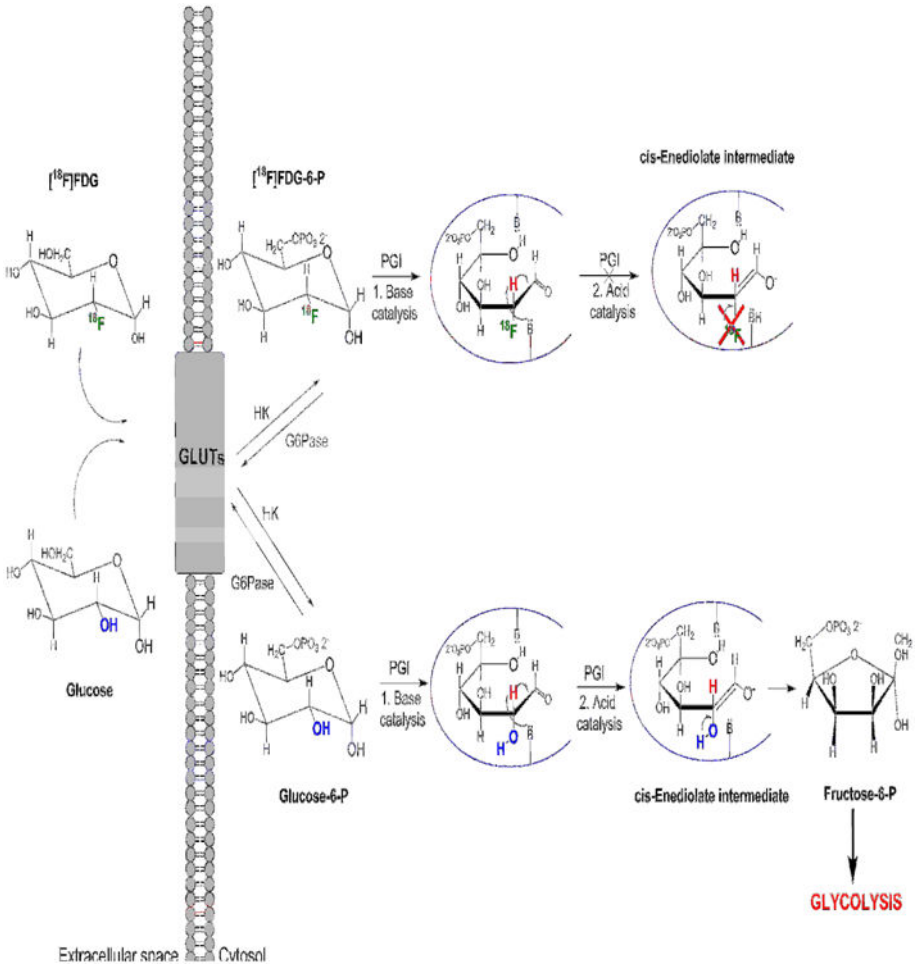


**Figure 2. Schematic representation of [$^{18}$F]FDG and glucose uptake and metabolisms**

[$^{18}$F]FDG is a glucose analog with $^{18}$F-fluorine replacing the oxygen in the C-2 position. [$^{18}$F]FDG is actively transported into the cytosol by the glucose transporters (GLUTs), which are overexpressed in pathological conditions such as cell transformation and inflammation. [$^{18}$F]FDG can then be phosphorylated by hexokinase (HK) to form [$^{18}$F]FDG-6-P, but cannot continue further the glycolytic pathway since the $^{18}$F substitution prevents the formation of [$^{18}$F]Fructose-6-P by phosphoglucose isomerase (PGI). Specifically the scheme demonstrates the inability of the $^{18}$F substituted cis-Enediolate intermediate to form a ring closure and thus the phosphorylated furanose ring.

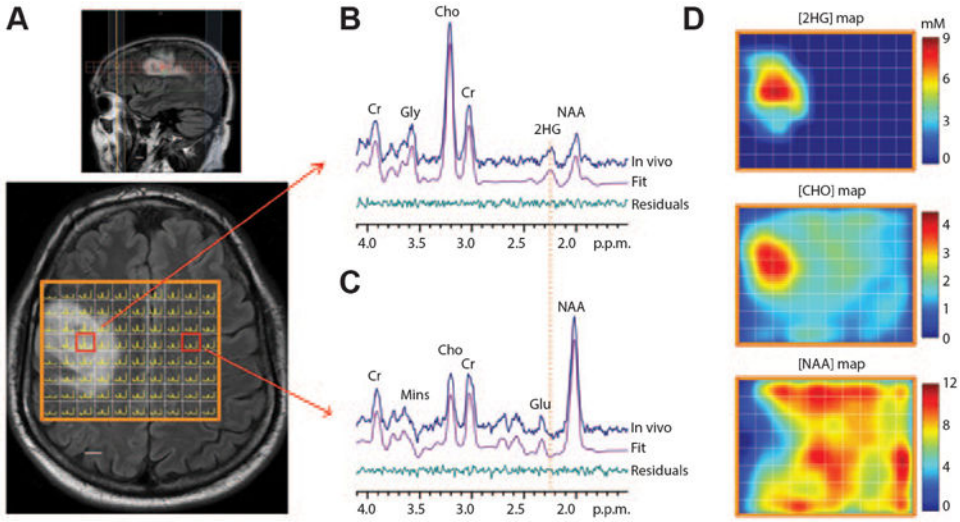


**Figure 3. Hyperpolarized magnetic resonance spectroscopy**

**(A)** General Electric (GE) SpinLab™ hyperpolarizer. Thermal and hyperpolarized spectra of $^{13}C$ pyruvate. A greater than 10,000 fold SNR enhancement of HP $^{13}C$ pyruvate compared to its thermal status is demonstrated. **(B)** (Top) Schematic representation of pyruvate to lactate conversion. (Bottom) Axial $T_2$-weighted MRI of a prostate cancer patient that received the highest dose of [1-$^{13}C$] pyruvate (0.43ml/kg) with corresponding metabolite image overlay of [1-$^{13}C$]lactate/[1-$^{13}C$] pyruvate ratio grater or equal to 0.6. (pink). The red arrows indicate a lesion originally observed in the anatomic MRI. *Adapted from S.J. Nelson et al.*[143]

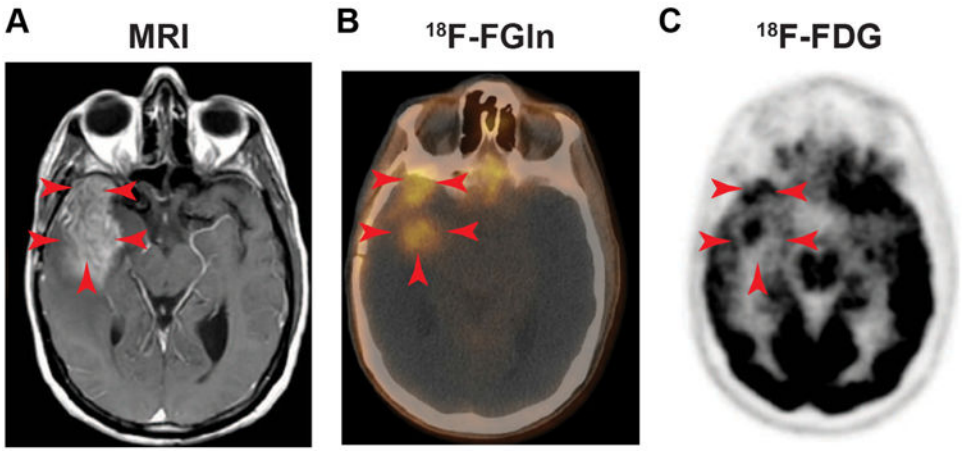


**Figure 4. [$^{18}$F] FGln shows uptake in human gliomas undergoing progression**

**(A)** DCE MRI of a patient with a Glioma showing gadolinium enhancement in the tumor area (red arrows). **(B)** Fusion [$^{18}$F]FGln PET-CT showing [$^{18}$F]FGln uptake in areas overlapping with the tumor. **(C)** Brain [$^{18}$F]FDG PET from the same patient displays high background brain and tumor uptake. *Adapted from S. Venneti et al*.[57]